LES of syngas/air turbulent nonpremixed jet flames at high pressure

P.P. Ciottoli[a,*], B. J. Lee[b], P.E. Lapenna[a], R. Malpica Galassi[a], M. Valorani[a], H. G. Im[b]

[a] *Sapienza University of Rome, Rome, Italy*
[b] *Clean Combustion Research Center, KAUST, Saudi Arabia*

Abstract

The pressure sensitivity of syngas/air turbulent non-premixed jet flames is inquired with a large eddy simulation (LES) approach. The software adopted to solve the reactive Navier-Stokes equations is developed within the OpenFOAM framework, using the YSLFM library for the flamelet-based chemical closure. The flamelet tabulation is obtained by means of an in-house code designed to solve unsteady flamelets of both ideal and real fluid mixtures. The validation of the numerical setup is attained by comparison of the numerical results with the Sandia/ETH-Zurich experimental database of the $CO/H_2/N_2$ non-premixed, unconfined, turbulent jet flame, referred to as flame-A. Three additional simulations, at pressure conditions of 2, 5 and 10 atm, are compared and analyzed to unravel computational and scientific challenges in characterizing turbulent flames at high pressures.

1. Introduction

The objective of this work is to numerically simulate turbulent non-premixed jet flames to investigate the effects of pressure on a syngas/air flame. This simulation campaign is aligned with the experimental effort in the Clean Combustion Research Center at KAUST, which is currently setting up a high pressure combustion test facility operating at up to 40 atm. The simulations will guide the experimental operating conditions and cross-validate the laser diagnostic measurements of various flame observables. The geometrical configuration is identical to the one adopted in the Sandia/ETH-Zurich $CO/H_2/N_2$ non-premixed unconfined turbulent jet flame, referred to as flame-A [1]. The first test case is carried out at ambient pressure, in order to validate the numerical results against the experimental data obtained in Sandia's Combustion Research Facility. The experimental data consist of: three-component velocity measurements [2], the major species concentrations (N_2,O_2,CO,H_2,CO_2,H_2O) obtained by combinations of spontaneous Raman scattering and Rayleigh scattering, OH and NO concentration measurements obtained by means of linear LIF. The same geometrical configuration and the same inflow velocity condition are employed to obtain simulations at 2, 5 and 10 atm. Given the Reynolds number of the inquired flows, which ranges between $1.67 \cdot 10^4$ at p =1atm and $1.67 \cdot 10^5$ at p=10atm, this study relies on a large eddy simulation (LES) approach for the turbulent closure problem, and on the steady laminar flamelet (SLF) method for the sub-grid chemical closure.

To the extent of the authors' knowledge, studies on the effects of pressure on this class of flames are not present in the open literature. Nonetheless, the Sandia flame-A experimental database has already been

*Corresponding author
Email address: pietropaolo.ciottoli@uniroma1.it (P.P. Ciottoli)

selected as benchmark for a comparative study of the steady and unsteady flamelet LES approaches [3], as well as for one dimensional turbulence (ODT) chemical closure model capabilities assessment [4]. The same flame configuration was numerically reproduced with a conditional moment closure (CMC) model and a transient flamelet model [5], with Eulerian particle flamelet model (EPFM) [6], fractal model (FM)[7], and transported PDF modeling [8].
First, the LES numerical framework is validated against the 1 atm Sandia flame-A experimental setup. Then, three additional simulations, at pressure conditions of 2, 5 and 10 atm, are compared and analyzed to unravel computational and scientific challenges in characterizing turbulent flames at high pressures

2. LES simulations

The reactive Navier-Stokes equations where numerically solved resorting to the OpenFOAM framework, using the YSLFM library for the flamelet-based chemical closure.

2.1. Numerical setup

The underlying finite-volume CFD solver is OpenFOAM 2.4 [9], a pressure-based (PISO), time-implicit segregated solver is used to solve the coupled mean momentum, pressure, and energy, equations using second-order spatial discretization. The chemical kinetics acting at small scales is modeled by means of steady laminar flamelet model (SLFM), which allows to model turbulence-chemistry interactions with large chemical kinetics mechanisms at a reasonable cost. The SLFM concept is based on the assumption that the flame in a turbulent flow can be regarded as an ensemble of thin laminar diffusion flames, generally referred to as flamelet, which are generated in a pre-processing step and stored in a flamelet look-up table. Thermodynamic properties and species mass fractions are then extracted from these tables using representative parameters, i.e. the mixture fraction $z(\boldsymbol{x}, t)$ and scalar dissipation rate $\chi(\boldsymbol{x}, t)$, whose spatial and temporal evolution is described in the physical space. The chemical mechanism employed is a detailed H2/CO mechanism with 12 species and 33 chemical reactions [10]. The flamelet tabulation is obtained by means of CSPTk toolkit, designed to solve unsteady flamelets of both ideal and real fluid mixtures [11]. The computational domain employed for the numerical computations is cylindrical, and the axial and radial domain sizes are 960 mm and 169 mm, respectively. The adopted computational mesh consists of approximately 7 million cells, with a resolution of about 1 mm in each direction. The inflow mean velocity condition is modeled as a fully-developed turbulent pipe flow profile, while the turbulent fluctuation magnitude is chosen according to the experimental measurements.

2.2. Validation

The validation of the numerical setup is attained by comparison of the numerical results with the Sandia/ETH-Zurich experimental database of the CO/H2/N2 non-premixed, unconfined, turbulent jet flame, referred to as flame-A [1]. The experiment is operated at ambient pressure, the fuel is injected at 292 K from a straight circular tube with squared-off ends with an inner diameter of 4.58 mm, and the outer diameter of 6.34 mm. The air coflow velocity is 0.75 m/s, it is wet (molar fraction of water 0.012) and has a temperature of 290 K. The fuel stream composition is 40/30/30 in CO/H2/N2 volume percentage. The choice of the inflow velocity condition requires an additional discussion. The experimental mean injection velocity is 76 m/s and the corresponding Reynolds number is 16700. The velocity profile employed as inflow condition corresponds to a fully developed turbulent pipe, i.e. $U(r) = U_{max} r^{1/n}$, where r is the injector pipe non dimensional inner radius, and U_{max} is the maximum velocity value. The first simulation campaign was carried out employing U_{max}=94.1m/s, matching the experimental mean injection velocity of 76 m/s. Discrepancies were found between numerical and experimental results, in terms of velocity, temperature

and mixture fraction spatial distribution. A second numerical simulation was carried out employing the same profile shape, but matching the experimental velocity profile, as shown in fig 1a. This second initial condition corresponds to a mean velocity of 84.7 m/s (U_{max} = 105.4m/s). A tentative explanation of this discrepancy may be found in the heat exchange between the injector post-tip and the fuel injected, where a high temperature on the post-tip would be coherent with the experimental observation [1] of a fully anchored flame. The axial and radial mean distributions of velocity, temperature, and mixture fraction are in

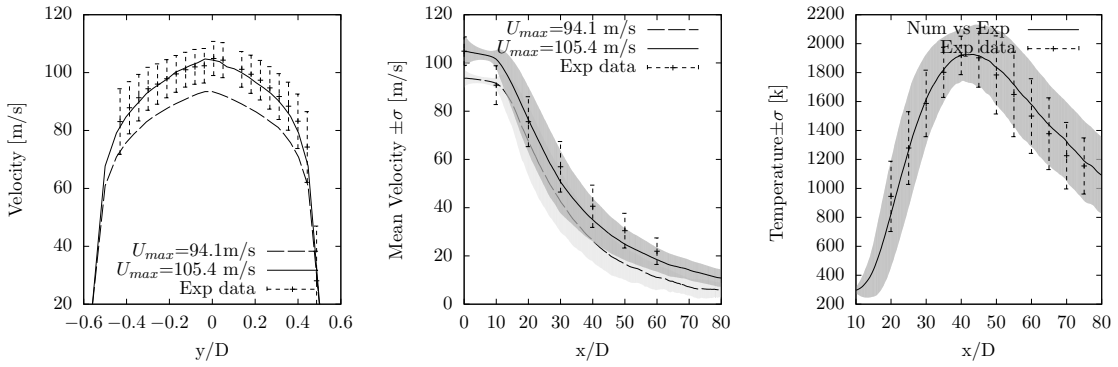

(a) Inflow velocity profile (b) Axial velocity distribution (c) Axial temperature distribution

Figure 1: Inflow velocity profile (a). Mean and standard deviation of the axial velocity distribution (b). Temperature (c). Numerical inflow matching mass flow rate (U_{max}=94.1m/s), numerical inflow matching mass flow rate (U_{max}=105.4m/s), and experimental data

very good agreement with the experimental results. In fig. 1c, are shown the mean values and the standard deviations of temperature. In fig. 2 the radial distribution of mean temperature and its standard deviation in x/D = 20 and x/D = 60 are compared to experimental measurements. An overall agreement of the mean quantities, also in terms of Y_{CO}, Y_{CO_2},Y_{OH}, Y_{H_2O} is observed (not shown).

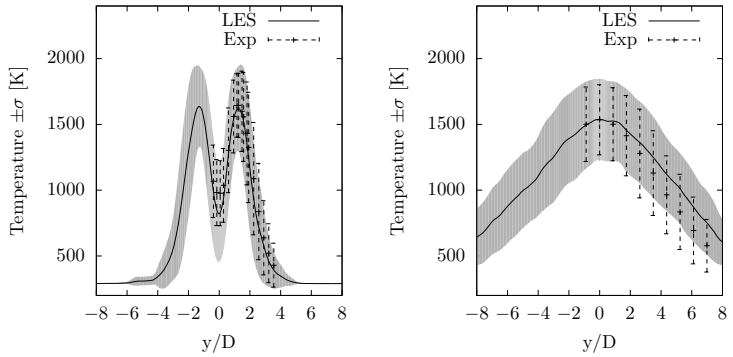

Figure 2: Radial distribution of temperature for x/D = 20 (left) and x/D = 60 (right)

2.3. Simulations at higher pressures

The same numerical setup was employed for three additional simulations for pressure values of 2, 5, and 10 atm. The same jet mean velocity of flame-A is selected, while the fully-developed turbulent pipe flow

velocity profile is modified according to the increased Reynolds number. Since the mean velocity is kept constant, and kinetic viscosity is independent on pressure, the pressure increase implies a linear Reynolds number increase through density. An increase in the Reynolds number results in a wider inertial subrange, and a smaller Kolmogorov scale. However, to directly resolve in space the same fraction of the inertial subrange in all the four simulations, the resulting computational mesh would have been too demanding in terms of computational resources. Hence, the mesh was kept identical in the various simulations, and the portion of turbulent kinetic energy modeled increases with pressure as discussed in the following. Both the instantaneous and mean temperature fields, for the four test cases are shown in fig. 3a.

The axial velocity, temperature, mixture fraction, and scalar dissipation mean values and their standard deviations are reported in fig. 4. The axial distribution of mean velocity and of its standard deviation result to be qualitatively similar, exhibiting an earlier velocity decrease in $x/D \approx 10$ and a lower standard deviation peak in $x/D = 20$, highlighting that the jet breakup occurs closer to the injector when pressure rises. Moreover, the temperature peak occurs further downstream for higher pressures, this being consistent with the mixture fraction axial distribution (not shown) which is convected further downstream for higher pressures.

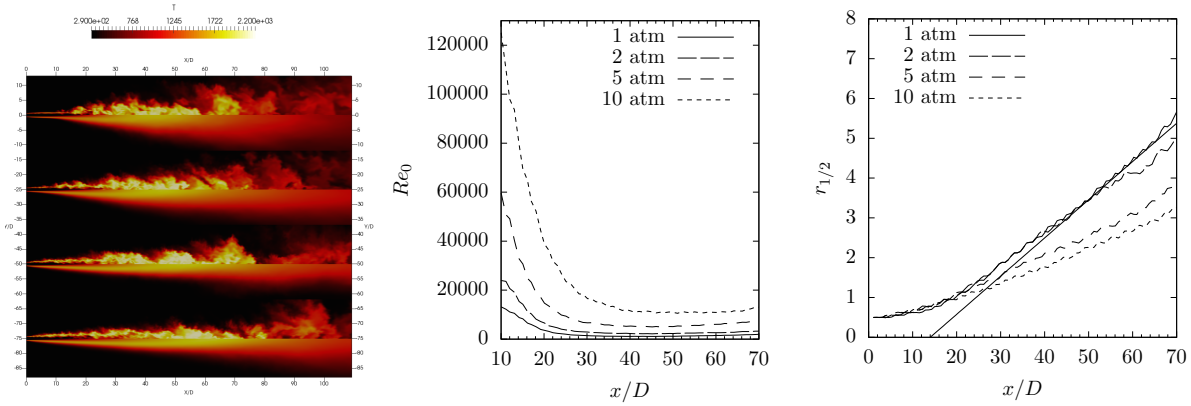

(a) Temperature (b) Re_x (c) $\mathrm{r}_{\frac{1}{2}}$

Figure 3: (a) Average and instantaneous temperature fields. From top to bottom p= 1, 2, 5, 10 atm. (b) Local Reynolds number Re_x. (c) Radial distance at which $\langle U \rangle = U_0/2$, $r_{1/2}$

A decrease in the maximum scalar dissipation rate axial distribution is observed. The mean scalar dissipation rate exhibits a peak for $x/D \approx 20$, which corresponds to the merging point of the inner sides of the round mixing layer originated from the injector postip recirculation region.

The mean and instantaneous scalar dissipation rate fields, $\widetilde{\chi}$ and $\langle \chi \rangle$, reveal that the scalar dissipation rate dependence on mixture fraction results to be bell-shaped centered in $Z = 0.5$ in the entire field, at all pressure values. Moreover the scalar dissipation decreases monotonically with x/D. A similar behavior is found for the scalar dissipation rate standard deviation, which exhibits a decrease with pressure. The scalar dissipation rate is here modeled as: $\chi = D|\nabla \widetilde{Z}|^2 + D_{sgs}\left(\frac{C_\chi}{2\Delta^2}\widetilde{Z''^2}\right)$, where D is the laminar diffusivity, D_{sgs} is the subgrid scale diffusivity, Δ is the local cell characteristic length, and $C_\chi = 2$. The second term, often modeled as $D_{sgs}|\nabla \widetilde{Z}|^2$, represents the sub-grid scale contribution to scalar dissipation. In particular, for a given computational mesh, because of the Reynolds increase with pressure, the portion of the turbulent energy contained in subgrid scale eddies increases, and the ratio $D_{sgs}/(D + D_{sgs})$ increases with pressure. The contribution of D_{sgs} is such that the ratio $D_{sgs}/(D + D_{sgs})$ is of order 0.1 for 1atm and reaches 0.5 at

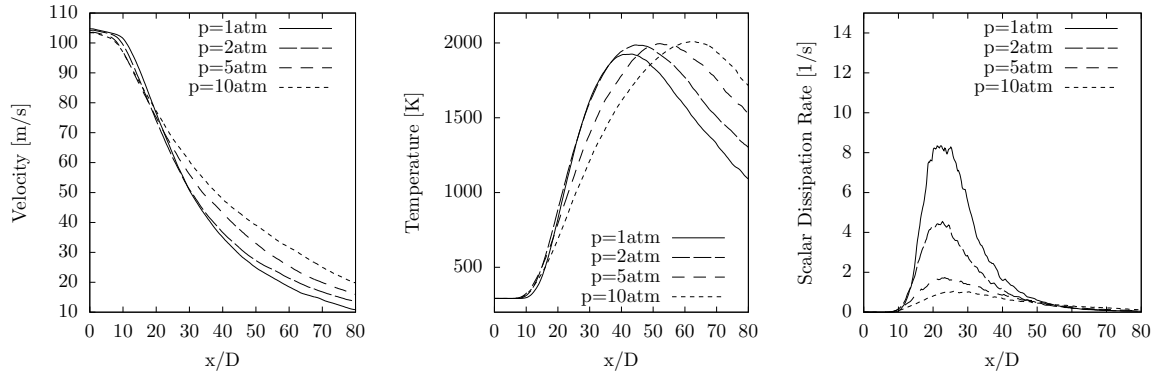

Figure 4: Mean velocity, temperature, and scalar dissipation axial distribution for p=1,2,5 and 10 atm.

10 atm. This reflects in the ratio $\widetilde{\chi_{sgs}}/\widetilde{\chi}$, whose average behavior is reported in fig. 5c, where it is shown how the $\widetilde{\chi_{sgs}}$ contribution is low, especially in the region close to the injector, where the highest values of $\widetilde{\chi}$ are observed. This leads to the conclusion that in the region close to the injector, the diminishing of the scalar dissipation with pressure is mainly ascribable to the decrease in the laminar diffusivity D. Also, the sensitivity of the composition on pressure is not too pronounced, exhibiting a diminution in the amount of H, OH, HCO, and H2O2 radical species (not shown).

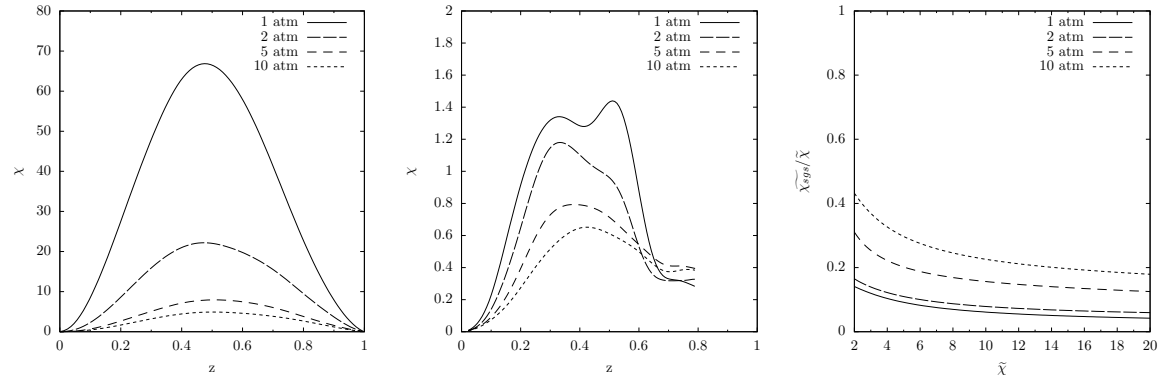

(a) $\langle\chi|Z\rangle$ at x/D=10 (b) $\langle\chi|Z\rangle$ at x/D=40 (c) $\widetilde{\chi_{sgs}}/\widetilde{\chi}$ VS $\widetilde{\chi}$

Figure 5: Conditional average of the scalar dissipation rate χ on the mixture fraction Z and pressure dependence of $\widetilde{\chi_{sgs}}/\widetilde{\chi}$ as function of $\widetilde{\chi}$.

Figure 3b shows the axial distribution of the local Reynolds number, $Re_0(x) = r_{1/2}(x)U_0(x)/\nu(x)$, where $U_0(x)$ and $r_{1/2}$ are the maximum velocity and radial distance at which $\langle U\rangle = U_0/2$ [12]. It is observed that, for higher pressures, the independence of Re_0 on x is recovered further downstream. In fig. 3c, $r_{1/2}$ is plotted as function of x/D, revealing that the jet spread angle $S \equiv dr_{1/2}/dx$ decreases with pressure, from values of 0.096 at p=1atm, which are in agreement with the well known experimental findings for cold flows, to values of 0.090 for p=10atm.

3. Conclusions

Large eddy simulations (LES) of turbulent nonpremixed jet flames were conducted to investigate the effects of pressure on the syngas/air flame behavior. The validation of the numerical setup is attained by comparison with the Sandia/ETH-Zurich flame-A. Three additional simulations, at pressure conditions of 2, 5 and 10 atm, are compared and analyzed highlighting a general decrease of the scalar dissipation. An increase of the jet flame length and a diminishing of the jet spread angle are observed. Although further investigations are required on the effects of pressure on chemical reactions, a decrease of radical species with pressure is observed.

Acknowledgements

The authors acknowledge the support of CCRC/KAUST (subaward agreement 1975-03 CCF) and of the Italian Ministry of University and Research (MIUR).

References

[1] R S Barlow, G J Fiechtner, C D Carter, M Flury, and Robert S Barlow. Sandia / ETH-Zurich CO/H2/N2 Flame Data - Release 1 . 1. *SAND chn Dccument 11*, pages 1–14, 2002.

[2] M. Flury. *Experimentelle Analyse der Mischungsstruktur in turbulenten nicht vorgemischten Flammen*. ETH Zurich Switzerland, 1999.

[3] S. Kim, S. Kang, and Y. Kim. Flamelet Modeling for Combustion Processes and NOx Formation in the Turbulent Nonpremixed CO/H2/N2 Jet Flames. *Combustion Science and Technology*, 168(1):47–83, 2001.

[4] J C Hewson and A R Kerstein. Stochastic simulation of transport and chemical kinetics in turbulent CO/H2/N2 flames. *Combustion Theory and Modelling*, 5(4):669–697, 2001.

[5] G Kim, S Kang, Y Kim, R W Bilger, and M J Cleary. Conditional moment closure and transient flamelet modelling for detailed structure and NOx formation characteristics of turbulent nonpremixed jet and recirculating flames. *Combustion Theory and Modelling*, 11(4):527–552, 2007.

[6] Seong Ku Kim and Yongmo Kim. Assessment of the Eulerian particle flamelet model for nonpremixed turbulent jet flames. *Combustion and Flame*, 154(1-2):232–247, 2008.

[7] E. Giacomazzi, F. R. Picchia, N. Arcidiacono, D. Cecere, F. Donato, and B. Favini. Unsteady simulation of a CO/H2/N2/air turbulent non-premixed flame. *Combustion Theory and Modelling*, 12(6):1125–1152, 2008.

[8] Xinyu Zhao, D. C. Haworth, and E. David Huckaby. Transported PDF Modeling of Nonpremixed Turbulent CO/H 2 /N 2 Jet Flames. *Combustion Science and Technology*, 184(5):676–693, 2012.

[9] H. Müller, F. Ferraro, and M. Pfitzner. Implementation of a Steady Laminar Flamelet Model for non-premixed combustion in LES and RANS simulations. *8th International OpenFOAM Workshop*, (JUNE):11–12, 2013.

[10] J.J. Scire J. Li, Z. Zhao, A. Kazakov, M. Chaos, F.L. Dryer. Kinetics of Acid Degradation of PPI in the presence of thiol. *International journal of chemical Kinetics*, 41:498–506, 2006.

[11] M. Valorani. Csptk- a software toolkit for the csp and tsr analysis of kinetic models and the simplification and reduction of chemical kinetics mechanisms. the software can be obtained upon request to m.valorani (mauro.valorani@uniroma1). 2015.

[12] Norbert Peters. *Turbulent Combustion:*. Cambridge University Press, Cambridge, 008 2000.